Tensile strained SiGe quantum well infrared photodetectors based on a light-hole ground state

P. Rauter, G. Mussler, D. Grützmacher, and T. Fromherz

Additional information on Appl. Phys. Lett.

Tensile strained SiGe quantum well infrared photodetectors based on a light-hole ground state

P. Rauter,[1,a)] G. Mussler,[2] D. Grützmacher,[2] and T. Fromherz[1]

[1]*Institute of Semiconductor and Solid State Physics, University of Linz, Altenberger Str. 69, 4040 Linz, Austria*

[2]*Peter-Grünberg Institut 9, Forschungszentrum Jülich, 52425 Jülich, Germany*

We report the fabrication and thorough characterization of tensile strained *p*-type SiGe quantum well infrared photodetectors (QWIPs) grown on a $Si_{0.74}Ge_{0.26}$ pseudosubstrate. The QWIPs operate from a light-hole (LH) ground state and feature responsivity peaks in both the terahertz and mid-infrared regimes with responsivity values up to 3.7 mA/W, originating from LH–LH, LH–heavy-hole, and LH–split-off-band transitions. © 2011 American Institute of Physics. [doi:10.1063/1.3593134]

The striving for the ultimate goal of a monolithic integrated silicon-based optoelectronic system continues to motivate comprehensive research efforts toward the realization of compatible detectors, emitters, and optical switches. Among the various approaches to overcome the weak interband absorption properties of bulk silicon itself are the employment of highly *n*-doped, tensile strained Ge (Ref. 1) or $Ge_{1-y}Sn_y$ (Ref. 2) layers featuring direct optical interband transitions, and the implementation of various intersubband device concepts, both in *n*- and *p*-type SiGe. While terahertz (THz) intraconduction band transitions in SiGe have recently been demonstrated[3] and *n*-type optoelectronic intersubband devices have not yet seen realization,[4] both intersubband electroluminescence emitters in the THz and mid-infrared (MIR) regions[5,6] and quantum well infrared photodetectors (QWIPs) operating in the MIR (Ref. 7) have been demonstrated in *p*-type SiGe. The intersubband devices realized in *p*-type SiGe so far are based on the confinement of holes in compressively strained QWs and therefore feature a heavy-hole (HH) ground state. Very recently, the possibility to grow QWIPs on a $Si_{1-y}Ge_y$ pseudosubstrate has tremendously increased the compositional parameter space accessible for intersubband device design.[7] In Ref. 8, Jiang *et al.* proposed the growth of a *tensile* strained QWIP on a $Si_{0.5}Ge_{0.5}$ pseudosubstrate, featuring a light-hole (LH) ground state. The obvious advantage of a LH-based QWIP lies in the reduced transport mass of the involved hole states as compared to compressively strained QWIPs, which inevitably involve the HH ground state in the detection process. Additionally, LH subbands feature a high in-plane effective mass, and thus an increased density of states, which once again increases the associated absorption coefficient. Therefore, intra-LH-band QWIPs are expected to exhibit larger optical dipole matrix elements and a higher density of states than compressively strained QWIPs and to feature superior responsivities at comparable detection wavelengths. However, up to now no intersubband device based on a tensile strained QW has been demonstrated.

We report the fabrication and thorough characterization of tensile strained *p*-type SiGe QWIPs. The presented QWIPs feature a LH ground state and exhibit responsivity

peaks both in the MIR and THz spectral regions.

The SiGe QWIP samples were grown pseudomorphically by molecular beam epitaxy on a $Si_{0.74}Ge_{0.26}$ [100] pseudosubstrate. The structures contain well layers composed of $Si_{0.78}Ge_{0.22}$, which are separated by 10 nm wide barrier layers of $Si_{0.9}Ge_{0.1}$. As confirmed by x-ray data, sample 1 features five 4.5 nm wide QWs and sample 2 includes ten 8.2 nm wide QWs, all of which are boron doped at a concentration of 1×10^{17} cm^{-3}. The Ge concentration of the well layers is *below* that of the pseudosubstrate, inducing tensile strain in the samples' active region, pushing the LH below the HH band edge and therefore enabling the QWIPs to operate from a LH ground state. The QW regions were sandwiched between a 300 nm thick bottom contact composed of *p*-doped (4×10^{17} cm^{-3}) $Si_{0.74}Ge_{0.26}$ and a 100 nm thick top contact layer of equal doping with a graded composition between $Si_{0.9}Ge_{0.1}$ at the QW region and $Si_{0.74}Ge_{0.26}$ on top of the sample. For vertical photocurrent (PC) measurements, the samples were processed into 900×900 μm^2 mesas and contacted by Al:Si metallization. In Fig. 1, the band structure of one period of the respective sample is shown for the HH, LH, and split-off (SO) bands. It was calculated using a six band *k.p* envelope function model for the valence bands, including strain according to Ref. 9. The band edges are
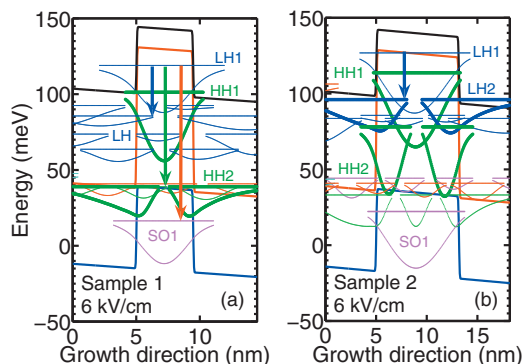
FIG. 1. (Color) Band structure. Plots (a) and (b) show the calculated LH, HH, and SO (black, red, blue) band edges at a field of 6 kV/cm and plots of the absolute squared wave functions at their eigenenergy values for samples 1 and 2, respectively. Optical LH–LH, LH–HH, and LH–SO transitions with dominant oscillator strengths are indicated by blue, green, and red arrows, respectively.

a)Electronic mail: patrick.rauter@jku.at.

98, 211106-1

shown as solid lines for the LH (black), HH (red), and SO (blue) bands together with the absolute squared wave functions at their respective eigenenergy values. As seen from Fig. 1, the ground state of each QW is formed by the LH1 state with a calculated energy separation from the lowest HH state of 20 meV and 12 meV in case of samples 1 and 2, respectively. As indicated by the HH band edge, the HH1 state is strongly bound, and is not expected to contribute to PC measurements. As shown by the band structure calculations for sample 2, a quasibound LH2 state [Fig. 1(b), bold blue wave function], separated by 30 meV from the LH1 ground state and thus energetically located close to the LH band edge, is calculated. In case of sample 1, on the other hand, the first excited LH state is a continuum state [Fig. 1(a), thin blue wave functions]. The HH2 state of sample 1 [Fig. 1(a), bold green wave function] exhibits a quasibound nature and is predicted to be energetically separated from the LH1 ground state by about 85 meV.

The LH-QWIPs' spectrally resolved responsivities were determined by Fourier transform infrared spectroscopic measurement of the PC. In order to determine the polarization dependence of the samples' responsivity, experiments were performed in two different modes of illumination. PC measurements were either performed under normal incidence on mesas featuring a frame-shaped metallization [transverse electric (TE), electric field parallel to sample surface], or on mesas completely covered by the top metallization by illuminating the active structure via side facets [transverse magnetic (TM), electric field parallel to growth direction]. For experiments in the THz range (up to 80 meV) performed in lock-in technique, the samples were cooled down to 5.9 K and illuminated by chopped globar radiation from a spectrometer equipped with a mylar beamsplitter. MIR measurements were performed at a sample temperature of 10 K, utilizing a KBr beamsplitter. The resulting PC spectra were normalized to the source spectrum. In order to quantitatively determine the QWIPs' responsivities, the spectra were calibrated by measuring the total current response to a chopped black-body radiation source at 200 °C and 500 °C, respectively. It shall be pointed out that in order to reach a maximum of reliability in the determined figures of merit, the MIR and THz spectra were calibrated *independently* by acquiring black-body induced current data in the THz as well as in the MIR cryostat.

Figure 2 shows the experimentally determined responsivity spectra of sample 1 at 0.5 V and for different polarizations. The sample exhibits a strong responsivity peak for TE polarized radiation around 85 meV, which can be clearly associated with the transition from the LH1 ground state to the quasibound HH2 state as indicated by the green arrow in Fig. 1(a). Remarkably, the responsivity peak originating from the LH1–HH2 transition is very narrow with a full width at half maximum of 30 meV, even though the final HH2 state is located high up in the LH continuum. This implies, that the quasibound nature of the HH2 state is not compromised by scattering processes into LH continuum states. The red dashed line in Fig. 2 shows the normalized absorption spectrum calculated from the simulated band structure for TE polarization, which resembles the measured responsivity spectrum with high accuracy. Due to selection rules and as predicted by the simulated absorption spectra for TE (dashed red line) and TM (dashed black line) polarized radiation in Fig. 2, the LH1–HH2 transition (green arrow in Fig. 1) is
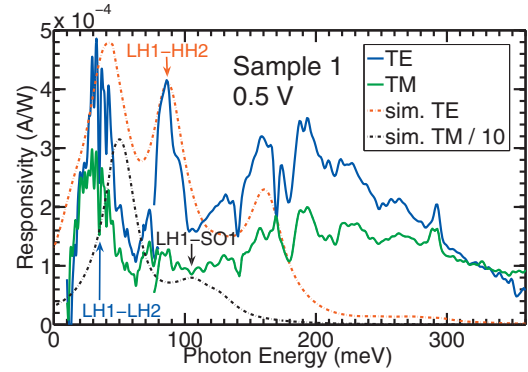

FIG. 2. (Color) Responsivity spectra of sample 1 and simulated absorption. The blue and green curves show the responsivity at a bias of 0.5 V for TE and TM polarized radiation, respectively. The TE spectrum shows two strong peaks around 35 meV and 85 meV, originating from LH–LH and LH–HH transitions, respectively. Note that the simulated absorption spectrum for TE polarized radiation (dashed red line) reproduces the measured responsivity with high accuracy. The LH1–HH2 transition is strong in TE polarization only, as predicted by the simulated TM absorption spectrum (dashed black line).

strong in TE polarization only, where it results in a responsivity peak value of 0.4 mA/W. The responsivity spectra of sample 1 exhibit an additional, strong peak around 35 meV, which can be attributed to transitions from the LH1 ground state into LH continuum states (blue arrow in Fig. 1). The responsivity peak originating from this intra-LH-band transition exhibits responsivities up to 0.45 mA/W, where no experimental demonstration of an optical intra-LH-transition has been reported in literature for any material system so far. As seen in Fig. 2, the LH1–LH2 transition is strong in *both* polarizations, a counterintuitive experimental observation, which is nevertheless predicted by the simulated absorption spectra represented by the dashed curves. However, the ratio between the measured peak responsivities for TE and TM polarized radiation originating from the LH1–LH2 transition deviates from the value predicted by simulations. While the calculated absorption of TM polarized radiation is by a factor of 7 *higher* than that for TE polarization, the measured TM responsivity is slightly *lower* than its TE counterpart. Most likely, the responsivity values determined experimentally for TM-polarized radiation are underestimated due to coupling losses during illumination via the sample's side facet. The strong intra-LH responsivity peak for TE polarization, which was also observed for sample 2 (not shown), might be due to the anisotropic dispersion of the LH band. It has to be stated, that the polarization dependence of the LH–LH transition requires further theoretical and experimental studies beyond the scope of this publication. However, a definite conclusion from the responsivity spectrum in Fig. 2 is, that *even for TE polarized radiation under normal incidence*, the LH–LH responsivity peak with a final state 10 meV above the LH band edge is slightly larger than the LH–HH peak with a quasibound final state. This can be attributed to the superior optical matrix element of LH–LH transitions as well as the high density of final states, as predicted in Ref. 8. As shown by the voltage series of measured MIR responsivity spectra in Fig. 3(a), at high applied voltages sample 1 exhibits a strong responsivity peak for TM polarized radiation around 110 meV, which reaches peak values of 3.7 mA/W. This peak can be identified with the LH1–SO1 transition, which is represented by the red arrow in Fig. 1(a) and is well predicted in
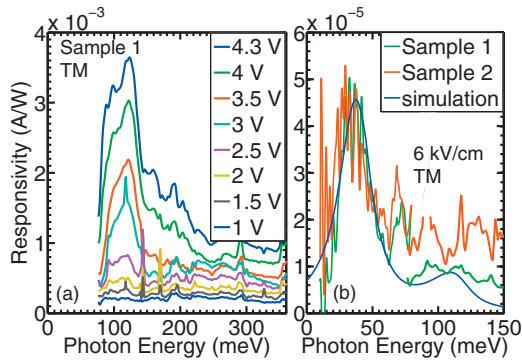
FIG. 3. (Color) LH1–SO1 responsivity of sample 1 (a) and THz spectra of samples 1 and 2 (b). The voltage series in (a) shows a strong responsivity peak evolving for sample 1 at high bias and for TM polarization, which is based on a LH1–SO1 transition. In (b), the green and red curves show the THz responsivity peaks at a low applied field of 6 kV/cm for samples 1 and 2, respectively. These peaks are based on LH–LH transitions, and are accurately reflected by the simulated absorption coefficient, as shown for sample 2 by the blue curve.

position and polarization dependence by the simulated absorption spectrum in Fig. 2. Up to now, no experimental observation of an optical LH–SO transition has been reported in literature. At low voltages, the SO1 state is strongly bound, as indicated by the simulation results in Fig. 1. Charge carriers excited into the SO1 state experience scattering into the bound LH1 and HH1 states before they are able to tunnel into the continuum and therefore do not contribute to the responsivity spectra at low bias in Fig. 2. As seen in Fig. 3(a), high voltages above 2 V are required to enable the efficient tunnelling of SO1 carriers into the continuum. This shows, that the strongly bound nature of the SO1 state is conserved despite its energetic location high up in the LH continuum.

The overall responsivity performance of sample 1 compares well to that of compressively strained SiGe QWIP devices (0.5 mA/W around 220 meV at 5 V bias[7]). Noise measurements indicate, that sample 1 features peak detectivities of at least 5.7×10^7 cm$\sqrt{\text{Hz}}$/W at 30 meV and a bias of 0.5 V. This low detectivity value originates from the small activation energies for dark-current due to the shallow QWs and the resulting strong dark-current of 0.12 μA. No SiGe THz QWIP has been reported in literature for comparison so far.

Figure 3(b) shows the responsivity spectrum of sample 2 for TM polarized radiation and at an applied field of 6 kV/cm (0.12 V), and compares it to the spectrum for sample 1 at an equal field (0.05 V). Note that the sharp fringes observed in the responsivity peaks of both samples are due to absorption by water vapor. The responsivity peak of sample 2 in the THz regime once again originates from an all-LH process, this time into a quasibound final state LH2, as indicated by the blue arrow in Fig. 1(b). As seen in Fig. 3(b), the respon-

sivity peak of sample 2 around 30 meV is slightly shifted toward lower energies as compared to the peak value of 35 meV for sample 1. This difference in the peak position is consistent with the band structure calculations presented in Fig. 1. The LH–LH transition of sample 2 features a quasi-bound final state located at the LH band edge, while the THz-response of sample 1 is based on transitions into LH continuum states above the band edge. The blue curve in Fig. 3(b) shows the absorption spectrum calculated for TM polarized radiation from the simulated band structure of sample 2, again resembling the measured responsivity well. The spectra in Fig. 3(b) imply that the LH–LH transitions of samples 1 and 2 lead to a THz responsivity peak of equal efficiency. Due to its design, apart from a broad response around 200 meV similar to that of sample 1 in Fig. 2, originating from transition into high continuum states at higher voltages, no sharp MIR responsivity features were experimentally observed for sample 2. Remarkably, both samples exhibit good responsivity values of 0.05 mA/W at extremely low fields down to 6 kV/cm (see Fig. 1).

In conclusion, we have demonstrated the fabrication and characterization of tensile strained SiGe valence band QWIPs operating from a LH ground state. The devices exhibit responsivity peaks of competitive values in the THz and MIR regimes, namely, around 30 meV (LH–LH, 0.3 mA/W at 0.5 V), 85 meV (LH–HH, 0.4 mA/W at 0.5 V), and 110 meV (LH–SO, 3.7 mA/W at 4.3 V). The experimental data indicate, that LH–LH intersubband transitions result in responsivity values superior to those based on LH–HH transitions. Thus, basing future optoelectronic SiGe devices on LH–LH transitions in tensile strained QWs offers the potential for performances superior to anything demonstrated on compressively strained, HH-based structures so far.

[1] J. Liu, X. Sun, R. Camacho-Aguilera, L. C. Kimerling, and J. Michel, Opt. Lett. **35**, 679 (2010).
[2] J. Mathews, R. T. Beeler, J. Tolle, C. Xu, R. Roucka, J. Kouvetakis, and J. Menéndez, Appl. Phys. Lett. **97**, 221912 (2010).
[3] M. De Seta, G. Capellini, Y. Busby, F. Evangelisti, M. Ortolani, M. Virgilio, G. Grosso, G. Pizzi, A. Nucara, and S. Lupi, Appl. Phys. Lett. **95**, 051918 (2009).
[4] K. Driscoll and R. Paiella, Appl. Phys. Lett. **89**, 191110 (2006).
[5] G. Dehlinger, L. Diehl, U. Gennser, H. Sigg, J. Faist, K. Ensslin, D. Grützmacher, and E. Müller, Science **290**, 2277 (2000).
[6] S. Lynch, R. Bates, D. Paul, D. Norris, A. Cullis, Z. Ikonic, R. Kelsall, P. Harrison, D. Arnone, and C. Pidgeon, Appl. Phys. Lett. **81**, 1543 (2002).
[7] P. Rauter, T. Fromherz, C. Falub, D. Grützmacher, and G. Bauer, Appl. Phys. Lett. **94**, 081115 (2009).
[8] L. G. Jiang, L. H. Kai, L. Cheng, C. S. Yan, and Y. J. Zhong, Semicond. Sci. Technol. **23**, 035011 (2008).
[9] T. Fromherz, E. Koppensteiner, M. Helm, G. Bauer, J. F. Nützel, and G. Abstreiter, Phys. Rev. B **50**, 15073 (1994).